

## D The WD40 Protein Caf4p is a Component of the Mitochondrial Fission Machinery and Recruits Dnm1p to Mitochondria

This chapter represents a further example of the use of MudPIT to analyze the polypeptide mixtures of moderate complexity resulting from affinity purified protein complexes. It was published as

Griffin, E. E., Graumann, J. and Chan, D. C. (2005). The WD40 protein Caf4p is a component of the mitochondrial fission machinery and recruits Dnm1p to mitochondria. *J Cell Biol*, 170(2):237–48.

The copyright is held by The Rockefeller University Press. This is an authorized reprint. Supplementary material is present at <http://www.jcb.org/cgi/content/full/jcb.200503148/DC1>.

### D.1 Abstract

The mitochondrial division machinery regulates mitochondrial dynamics and consists of Fis1p, Mdv1p, and Dnm1p. Mitochondrial division relies on the recruitment of the dynamin-related protein Dnm1p to mitochondria. Dnm1p recruitment depends on the mitochondrial outer membrane protein Fis1p. Mdv1p interacts with Fis1p and Dnm1p, but is thought to act at a late step during fission because Mdv1p is dispensable for Dnm1p localization. We identify the WD40 repeat protein Caf4p as a Fis1p-associated protein that localizes to mitochondria in a Fis1p-dependent manner. Caf4p interacts with each component of the fission apparatus: with Fis1p

and Mdv1p through its NH<sub>2</sub>-terminal half and with Dnm1p through its COOH-terminal WD40 domain. We demonstrate that *mdv1*Δ yeast contain residual mitochondrial fission due to the redundant activity of Caf4p. Moreover, recruitment of Dnm1p to mitochondria is disrupted in *mdv1*Δ *caf4*Δ yeast, demonstrating that Mdv1p and Caf4p are molecular adaptors that recruit Dnm1p to mitochondrial fission sites. Our studies support a revised model for assembly of the mitochondrial fission apparatus.

## D.2 Introduction

Mitochondria are dynamic organelles that undergo fusion and fission. These processes intermix the mitochondria within cells and control their morphology. In addition to controlling mitochondrial shape, recent studies have also implicated components of the fission machinery in regulation of programmed cell death (Frank et al. 2001; Fannjiang et al. 2004; and Jagasia et al. 2005). Genetic approaches in *Saccharomyces cerevisiae* have identified *DNM1*, *FIS1*, and *MDV1* as components of the mitochondrial fission pathway (Shaw and Nunnari 2002). Dnm1p and its mammalian homologue Drp1 are members of the extensively studied dynamin family of large, oligomeric GTPases. Although the precise mechanism remains controversial, dynamins may couple GTP hydrolysis to a conformational constriction that causes membrane scission (Praefcke and McMahon 2004). In yeast cells, Dnm1p dynamically localizes to dozens of puncta that are primarily associated with mitochondria (Otsuga et al. 1998; Bleazard et al. 1999; Sesaki and Jensen 1999; and Legesse-Miller et al. 2003). A subset of these puncta are sites of future fission.

The assembly of functional Dnm1p complexes on mitochondria is a critical issue in understanding the mechanism of mitochondrial fission. The mitochondrial outer membrane protein Fis1p is required for the formation of normal Dnm1p puncta on mitochondria. In *fis1* $\Delta$  cells, Dnm1p puncta are primarily cytosolic or form abnormally large aggregates on mitochondria (Otsuga et al. 1998; Bleazard et al. 1999; Sesaki and Jensen 1999; and Legesse-Miller et al. 2003). Mdv1p interacts with Fis1p through its NH<sub>2</sub>-terminal half and with Dnm1p through its COOH-terminal WD40 domain. However, Mdv1p appears dispensable for Dnm1p assembly on mitochondria because *mdv1* $\Delta$  cells show little or no change in Dnm1p localization, even though mitochondrial fission is disrupted (Fekkes et al. 2000; Tieu and Nunnari 2000; Tieu et al. 2002; and Cervený and Jensen 2003). These observations have led to two important features of a recently proposed model for mitochondrial fission (Shaw and Nunnari 2002; Tieu et al. 2002; and Osteryoung and Nunnari 2003). First, Fis1p acts to assemble and distribute Dnm1p on mitochondria in an Mdv1p-independent step. Second, Mdv1p acts downstream of Dnm1p localization to stimulate membrane scission. An alternative model proposes that Dnm1p marks the site of mitochondrial fission and recruits Fis1p and Mdv1p into an active fission complex (Shaw and Nunnari 2002; Tieu et al. 2002; and Osteryoung and Nunnari 2003). Again, in this model Mdv1p functions downstream of Dnm1p localization.

Despite extensive efforts, however, there is no evidence that Fis1p can interact directly with Dnm1p. We speculated that there may be an additional component of the mitochondrial fission pathway required for the Fis1p-dependent assembly of Dnm1p puncta on mitochondria. Because a genome-wide screen for mitochondrial morphology mutants (Dimmer et al. 2002) did not yield obvious candidates, we used a biochemical approach to identify additional components of the mitochondr-

ial fission machinery. Using immunopurification and mass spectrometry, we have identified the WD40 repeat protein Caf4p as a Fis1p–interacting protein. Caf4p localizes to mitochondria and associates with Fis1p, Mdv1p, and Dnm1p. Moreover, we show that *mdv1*Δ cells are only partially deficient in mitochondrial fission due to the redundant activity of Caf4p. Importantly, Caf4p mediates recruitment of Dnm1p puncta to mitochondria in *mdv1*Δ yeast. Inclusion of *CAF4* significantly clarifies the current models for mitochondrial fission.

## D.3 Results

### D.3.1 Caf4p is Associated with Fis1p

To identify Fis1p–associated proteins by multidimensional protein identification technology (MudPIT) (Dimmer et al. 2002), we constructed a yeast strain containing endogenous Fis1p with an NH<sub>2</sub>–terminal tandem affinity tag (fig. D.1A). NH<sub>2</sub>–terminal tagging is necessary because *FIS1* is nonfunctional when COOH–terminally tagged (unpublished data). We first designed a recombination cassette containing 9×Myc/TEV/*URA3*/TEV/His<sub>8</sub> modules (fig. D.1A). After targeted integration into the *FIS1* locus, spontaneous and precise recombination between the flanking ≈ 50 bp tobacco etch virus (TEV) protease sites excises *URA3*. This strategy was used to generate a yeast strain (DCY 1557) that expresses a functional Fis1p with an NH<sub>2</sub>–terminal 9×Myc/TEV/His<sub>8</sub> tag (M<sub>9</sub>TH–Fis1p) from the endogenous locus.

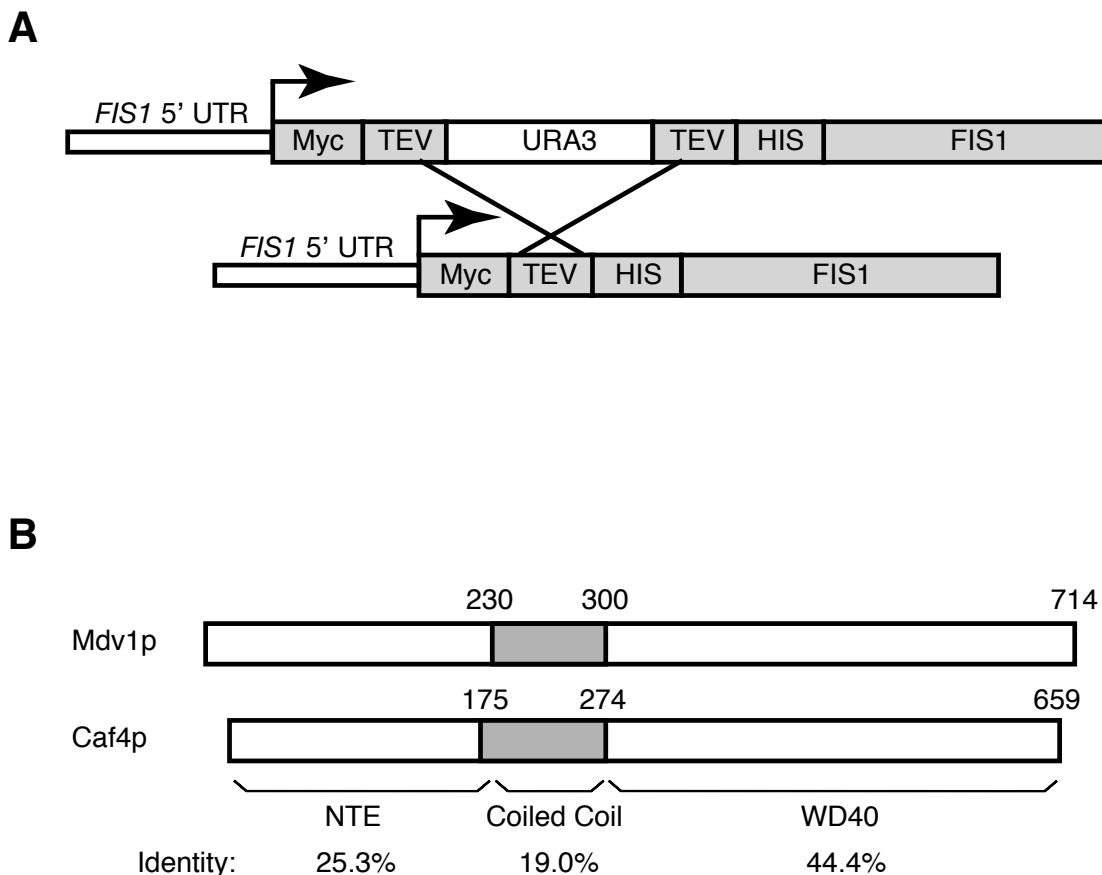


**Figure D.1 Construction of M<sub>9</sub>TH-*FIS1* and Caf4p/Mdv1p Alignment.** (A) A 9×Myc-TEV-*URA3*-TEV-His<sub>8</sub> cassette was PCR amplified with *FIS1*-targeting primers and integrated in-frame into the NH<sub>2</sub>-terminus of *FIS1*. Pop-out of the *URA3* cassette by recombination between flanking TEV sites yielded M<sub>9</sub>TH-*FIS1* under the control of the endogenous *FIS1* promoter. UTR: untranslated region. (B) Schematic of Mdv1p and Caf4p. The NH<sub>2</sub>-terminal extension (NTE), coiled-coil, and WD40 regions are shown with percent identity. Overall identity is 37 and overall similarity is 57.

Tandem affinity-purified M<sub>9</sub>TH-Fis1p was subjected to MudPIT analysis in two independent experiments (see materials and methods). Fis1p was identified in both experiments (61.3% coverage, 14 unique peptides; 58.7% coverage, 9 unique peptides). Mdv1p, a previously identified member of the mitochondrial fission pathway and a known Fis1p-interacting protein, was also identified in both experiments (21.1% coverage, 12 unique peptides; 10.2% coverage, 5 unique peptides). These

data confirmed that our MudPIT procedure could preserve and identify Fis1p complexes relevant to mitochondrial fission. Dnm1p was not observed in either dataset, in agreement with previous immunoprecipitation experiments (Mozdy et al. 2000). The complete datasets are presented in Table S1 (available at <http://www.jcb.org/cgi/content/full/jcb.200503148/DC1>).

Interestingly, peptides derived from the WD40 repeat protein Caf4p were identified in both Fis1p MudPIT experiments (24.4% coverage, 9 unique peptides; 8.5% coverage, 3 unique peptides). *CAF4* (YKR036C) was first identified in a yeast two-hybrid screen for CCR4p-interacting proteins (Liu et al. 2001). CCR4p is a central component of the CCR4–NOT transcriptional regulator and cytosolic deadenylase complex (Denis and Chen 2003). Caf4p is the nearest homologue of Mdv1p in *S. cerevisiae* (38% identity and 57% similarity), and the two proteins show extensive sequence identity throughout their lengths (fig. D.1B). Both proteins share a unique NH<sub>2</sub>-terminal extension (NTE; 25.3% identity), a central coiled-coil (CC) domain (19% identity) and a COOH-terminal WD40 repeat domain (44.4% identity). The Caf4p CC scores significantly more weakly ( $\approx 0.3$  probability) than the Mdv1p coiled coil ( $\approx 1.0$  probability) in the MultiCoil prediction program (Wolf et al. 1997).

### D.3.2 Caf4p Interacts with Components of the Mitochondrial Fission Machinery

We sought independent confirmation of the physical interaction between Fis1p and Caf4p. For immunoprecipitation experiments, Caf4p–HA or Mdv1p–HA were expressed from their endogenous promoters in strains carrying chromosomal M<sub>3</sub>TH–*FIS1* (3×Myc/TEV/His<sub>8</sub>–*FIS1*) and deleted for *CAF4* or *MDV1*, respectively. When

M<sub>3</sub>TH–Fis1p was immunoprecipitated,  $\approx 5\%$  of both Caf4p–HA and Mdv1p–HA coprecipitated (fig. D.2A, lanes 7 and 10).

Previous yeast two–hybrid analysis determined that the NTE/CC region of Mdv1p (residues 1–300) is responsible for its interaction with Fis1p (Tieu et al. 2002). We detected the same interaction by coimmunoprecipitation (fig. D.2A, lane 11). Additionally, we found that the analogous region of Caf4p (residues 1–274) also interacted with Fis1p (fig. D.2A, lane 8). A shorter Caf4p fragment lacking the majority of the predicted coiled coil (residues 1–250) interacted equally well with Fis1p (unpublished data). In contrast, Fis1p did not bind to the COOH–terminal regions of either Mdv1p or Caf4p (fig. D.2A, lanes 9 and 12). These data suggest that both Caf4p and Mdv1p likely interact with Fis1p through a common mechanism involving the NTE domain.

We also used a yeast two–hybrid assay to analyze the interaction of Caf4p and Mdv1p with Fis1p and Dnm1p (Table D.8). Full–length Caf4p and an NTE/CC fragment of Caf4p interacted strongly with the cytosolic portion of Fis1p (residues 1–128), consistent with our immunoprecipitation data. Similar interactions were observed between Fis1p and both full–length Mdv1p and the NTE/CC region of Mdv1p, as has been previously reported (Tieu et al. 2002; and Cerveny and Jensen 2003). The WD40 domain of both Mdv1p and Caf4p interacted strongly with Dnm1p. However, full–length Mdv1p interacted more weakly and an interaction between full–length Caf4p and Dnm1p was not detected. These results suggest that the interaction of the WD40 domain with Dnm1p is regulated and may be inhibited by the NH<sub>2</sub>–terminal region of Caf4p and Mdv1p.

We also detected homotypic and heterotypic interactions between Caf4p and Mdv1p. Approximately 5% of Caf4p–HA and Caf4p–N–HA (residues 1–274), but

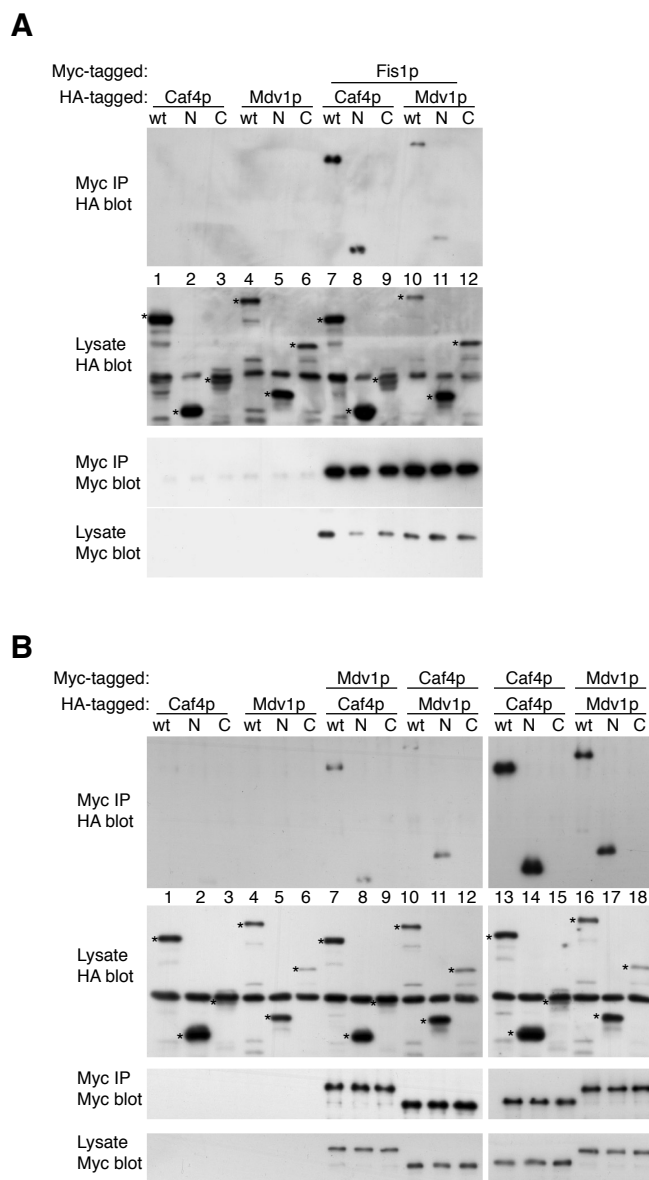


**Figure D.2 Caf4p and Mdv1p Coimmunoprecipitation Experiments.** (A) Yeast carrying the indicated HA- and Myc-tagged constructs were lysed and immunoprecipitated with an anti-Myc antibody. Total lysates (labeled “Lysate”) and immunoprecipitated samples (labeled “Myc IP”) were analyzed by immunoblotting with anti-Myc (9E10) and anti-HA (12CA5) antibodies as indicated. The expression constructs were: Caf4p wt (residues 1–659), Caf4p N (residues 1–274), Caf4p C (residues 275–659), Mdv1 wt (residues 1–714), Mdv1p N (residues 1–300), and Mdv1p C (residues 301–714). The yeast backgrounds were: (A) wild-type, lanes 1–6; *caf4* $\Delta$  M<sub>3</sub>TH-*FIS1*, lanes 7–9; *mdv1* $\Delta$  M<sub>3</sub>TH-*FIS1*, lanes 10–12; (B) wild-type, lanes 1–6; *caf4* $\Delta$  MDV1-HTM, lanes 7–9; *mdv1* $\Delta$  CAF4-HTM, lanes 10–12; CAF4-HTM, lanes 13–15; MDV1-HTM, lanes 16–18. (B) Yeast carrying the indicated HA- and Myc-tagged constructs were immunoprecipitated and analyzed as in A. Immunoprecipitated samples were loaded at 10 (A) and 20 (B) equivalents of the lysate samples. HA-tagged proteins in the lysate are marked with an asterisk. The HA-tagged Caf4p C polypeptide comigrates with a background band in the total lysate blot probed with HA antibody.



**Table D.8 Caf4p and Mdv1p Interact With Dnm1p and Fis1p in a Yeast Two-hybrid Assay.** Caf4p, Mdv1p, Fis1p, and Dnm1p fragments were scored for growth (+), no growth (−), or poor growth (weak) on adenine-deficient plates. All constructs showed no growth when paired with empty activation domain or DNA-binding domain vector. Binding domain fusions are listed across the top of the table and activation domain fusions are listed down the left. Caf4p and Mdv1p N and C fragments are defined in fig. D.2.

		Fis1p	Dnm1p	Caf4p			Mdv1p		
				wt	N	C	wt	N	C
Fis1p		−	−	+	+	−	+	+	−
Dnm1p		−	+	−	−	−	−	−	−
Caf4p	wt	+	−	−	−	−	−	weak	−
	N	+	−	−	−	−	−	−	−
	C	−	+	−	−	−	−	−	−
Mdv1p	wt	+	+	−	+	−	+	+	−
	N	+	−	−	+	−	+	+	−
	C	−	+	−	−	−	−	−	−

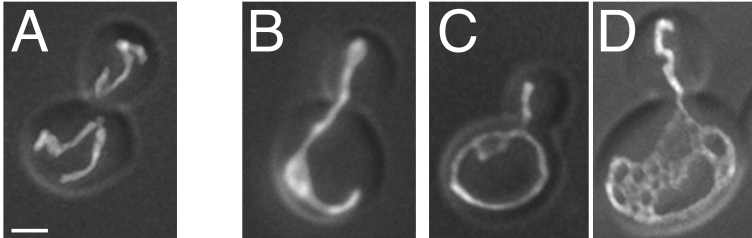
not Caf4-C-HA (residues 275–659), coimmunoprecipitate with full-length Caf4p-HTM (fig. D.2B, lanes 13–15). A similar level of Mdv1p-HA and Mdv1p-N-HA (residues 1–300), but not Mdv1-C-HA (residues 301–714), coimmunoprecipitated with Mdv1p-HTM (fig. D.2B, lanes 16–18). When Caf4p-HTM was precipitated,  $\approx 1\%$  of Mdv1p-HA and Mdv1p-N-HA, but not Mdv1p-C-HA, coprecipitated (fig. D.2B, lanes 10–12). Similarly, when Mdv1p-HTM was precipitated,  $\approx 1\%$  of Caf4p-HA and Caf4p-N-HA, but not Caf4p-C-HA, coprecipitated (fig. D.2B, lanes 7–9). Moreover, the NTE/CC regions of Caf4p and Mdv1p interact in the two-hybrid assay (Table D.8). Therefore, Caf4p interacts with all three members of the fission pathway, with the NH<sub>2</sub>-terminal region mediating interactions with Fis1p, Mdv1p, and homotypic interactions with Caf4p.

### D.3.3 Caf4p is Involved in Mitochondrial Division

Given that Caf4p interacts with Fis1p, Mdv1p, and Dnm1p, we hypothesized that

Caf4p, like Mdv1p, is a component of the mitochondrial division apparatus. *caf4* $\Delta$  yeast, however, display normal mitochondrial morphology, with tubular mitochondria evenly dispersed around the cell cortex (fig. D.3). Wild-type mitochondrial morphology was also observed at elevated temperatures and on carbon sources other than dextrose (glycerol or galactose; unpublished data). This observation is not surprising, given that *CAF4* was not identified in a genome-wide screen of deletion strains for mitochondrial morphology mutants (Dimmer et al. 2002).

We next tested whether *caf4* $\Delta$  cells show synthetic defects in mitochondrial morphology when other components of the fission machinery are deleted. Yeast defective in mitochondrial fission display net-like mitochondrial morphology due to unopposed mitochondrial fusion (Bleazard et al. 1999; and Sesaki and Jensen 1999). These mitochondrial nets can have a spread morphology (fig. D.33, C and D), or they can collapse to one side of the cell (fig. D.3B). Although *FIS1*, *DNM1*, and *MDV1* are all involved in mitochondrial fission, we found that *mdv1* $\Delta$  cells have a distribution of mitochondrial profiles that can be readily distinguished from both *fis1* $\Delta$  and *dnm1* $\Delta$  cells (fig. D.3). In rich dextrose medium, almost all *fis1* $\Delta$  or *dnm1* $\Delta$  cells (93 % and 90 %, respectively) contain collapsed mitochondrial nets. In contrast, less than half of *mdv1* $\Delta$  cells contain collapsed nets, with the majority displaying a spread net morphology. The spread nets range in morphology from interconnected tubules with several loops (fig. D.3C) to networks with complex fenestrations (fig. D.3D). *mdv1* $\Delta$  *dnm1* $\Delta$  cells behave identically to *dnm1* $\Delta$  cells, with > 90 % collapsed nets in dextrose (fig. D.3). This observation indicates that the *dnm1* $\Delta$  collapsed net phenotype is epistatic to the *mdv1* $\Delta$  spread net phenotype. In rich galactose medium (unpublished data), a greater portion of all strains contain spread nets, but again *mdv1* $\Delta$  cells have a higher percentage of cells with spread



Genotype	Wild-type	Collapsed net	Spread net
Wild-type	100	0	0
<i>caf4</i> $\Delta$	100	0	0
<i>mdv1</i> $\Delta$	0	45.5	54.5
<i>dnm1</i> $\Delta$	0	90	10
<i>fis1</i> $\Delta$	0	92.5	7.5
<i>mdv1</i> $\Delta$ <i>caf4</i> $\Delta$	0	91.5	8.5
<i>mdv1</i> $\Delta$ <i>dnm1</i> $\Delta$	0	91.5	8.5

**Figure D.3** *CAF4* Regulates Mitochondrial Morphology. Strains expressing mitochondrially targeted GFP were grown in YP dextrose to mid-log phase and fixed. The percentage of cells ( $n = 400$ ) with mitochondria having wild-type (A), collapsed net (B), or spread net morphology (C and D) is tabulated. The spread net phenotype encompasses a distribution of morphologies ranging from simple structures containing one or two loops (C) to complexly fenestrated mitochondria with dozens of loops (D). For both wild-type and *caf4* $\Delta$  strains, the wild-type category includes 1% fragmented cells. Bar, 1  $\mu\text{m}$ .

nets (80%) compared with *fis1* $\Delta$  (45.5%), *dnm1* $\Delta$  (53%), or *mdv1* $\Delta*dnm1* $\Delta$  cells (40.5%). These results agree with a previous report that *mdv1* $\Delta$  cells have more spread nets compared with *dnm1* $\Delta$  cells in galactose medium (Cervený et al. 2001). However, this study found that the *mdv1* $\Delta$  spread net phenotype is epistatic to the *dnm1* $\Delta$  collapsed net phenotype (Cervený et al. 2001). The reason for this$

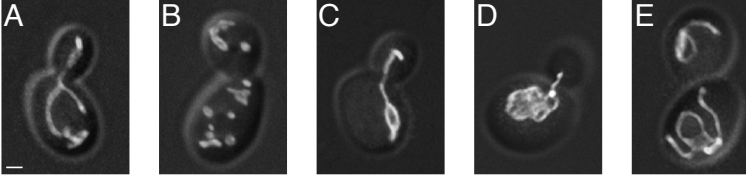
discrepancy is unclear, but we note the *mdv1* $\Delta$  morphology is most distinct in dextrose cultures.

Most interestingly, we found that *mdv1* $\Delta$  *caf4* $\Delta$  cells have mitochondrial net distributions indistinguishable from either *dnm1* $\Delta$  cells or *fis1* $\Delta$  cells. Deletion of *CAF4* in *mdv1* $\Delta$  cells markedly shifts the distribution to one composed almost entirely of collapsed mitochondrial nets (> 90% in dextrose, fig. D.3). Our results support a model in which partial reduction of mitochondrial fission results in predominantly spread mitochondrial nets, and complete loss of fission eventually results in collapse of the nets. That is, *mdv1* $\Delta$  cells retain residual mitochondrial fission, whereas *mdv1* $\Delta$  *caf4* $\Delta$  cells are devoid of fission, similar to *dnm1* $\Delta$ , *fis1* $\Delta$ , or *mdv1* $\Delta$  *dnm1* $\Delta$  cells. An analogous situation appears to exist in mammalian cells, in which weak Drp1 dominant-negative alleles cause the formation of spread nets, whereas strong dominant-negative alleles cause nets to collapse (Cervený et al. 2001).

We tested this model by reanalyzing mitochondrial morphologies in the presence of latrunculin A, which disrupts the actin cytoskeleton. Disruption of the actin cytoskeleton leads to rapid fragmentation of the mitochondrial network due to ongoing mitochondrial fission (Boldogh et al. 1998; and Jensen et al. 2000). Latrunculin A treatment rapidly resolves a fraction of collapsed nets into spread nets (Jensen et al. 2000; and Cervený et al. 2001), and allows a closer examination of the degree of connectivity in mitochondrial nets. Similarly, in mammalian cells, collapsed mitochondrial nets induced by overexpression of dominant-negative Drp1 can be spread by the microtubule-depolymerizing agent nocodazole (Smirnova et al. 2001). Both wild-type and *caf4* $\Delta$  yeast treated with latrunculin A show mitochondrial fragmentation (fig. D.4). 80% of *mdv1* $\Delta$  cells treated with latrunculin A contain partial

mitochondrial nets (fig. D.4E, partial net) that are less interconnected and have fewer fenestrations than the collapsed or spread nets that predominate in latrunculin A-treated *dnm1* $\Delta$  or *fis1* $\Delta$  cells. 95% of latrunculin A-treated *mdv1* $\Delta$  *caf4* $\Delta$  cells show either collapsed nets or highly fenestrated spread nets, a profile indistinguishable from that in *dnm1* $\Delta$  or *fis1* $\Delta$  cells (fig. D.4). Thus, after disruption of the actin cytoskeleton, *mdv1* $\Delta$  yeast display a distribution of mitochondrial morphologies that suggest an incomplete defect in mitochondrial fission. In contrast, *mdv1* $\Delta$  *caf4* $\Delta$  yeast have mitochondrial morphologies similar to that in *fis1* $\Delta$  and *dnm1* $\Delta$  yeast. We conclude that *CAF4* mediates low levels of mitochondrial fission in *mdv1* $\Delta$  cells.

We next monitored the mitochondrial network in *mdv1* $\Delta$  cells by time-lapse microscopy to assess the levels of mitochondrial fission. In pilot experiments, we found that free mitochondrial ends produced by fission events in *mdv1* $\Delta$  cells were rapidly involved in fusion events, making unambiguous documentation of fission difficult. Because latrunculin A reduces the levels of fusion and thereby should prolong the presence of free mitochondrial ends, we monitored mitochondrial dynamics in latrunculin A-treated *mdv1* $\Delta$  cells carrying the outer membrane marker OM45-GFP. In 8 out of 10 *mdv1* $\Delta$  cells, we observed at least one fission event in a 30 min recording period (fig. D.4, F-H; videos 1 and 2, available at <http://www.jcb.org/cgi/content/full/jcb.200503148/DC1>). Due to the complexity and rapid rearrangements of the mitochondrial networks in these cells (see videos 1 and 2), these numbers likely underestimate the actual levels of fission. In contrast, no fission events were observed in 8 *mdv1* $\Delta$  *caf4* $\Delta$  cells. We conclude that the ability of *CAF4* to mediate mitochondrial fission events contributes significantly to the spread net morphology of *mdv1* $\Delta$  cells.



Genotype	LatA treatment	Wild-type	Fragments and short tubules	Collapsed net	Spread net	Partial net
Wild-type	-	95	5	0	0	0
	+	8	92	0	0	0
<i>caf4</i> Δ	-	95	4.5	0	0	0.5
	+	8.5	91.5	0	0	0
<i>mdv1</i> Δ	-	0	0	45.5	50.5	4
	+	0	0	5.5	14.5	80
<i>dnm1</i> Δ	-	0	0	96	3.5	0.5
	+	0	0	32.5	63.5	4
<i>fis1</i> Δ	-	0	0	96	4	0
	+	0	0	36.5	58.5	5
<i>mdv1</i> Δ <i>caf4</i> Δ	-	0	0	95	4	1
	+	0	0	38.5	57	4.5
<i>mdv1</i> Δ <i>dnm1</i> Δ	-	0	0	95	4.5	0.5
	+	0	0	26	70.5	3.5

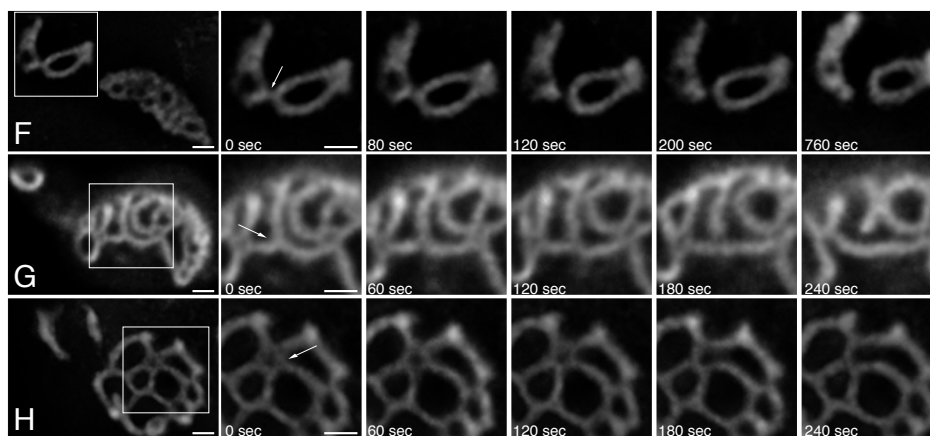


**Figure D.4** *CAF4* Mediates Residual Fission in *mdv1*Δ Cells. Top: mid-log cultures grown in YP dextrose were treated for 60 min with 200 μM latrunculin A (+) or vehicle (-). For each strain, 200 cells were scored into the following phenotypic categories: wild-type (A), fragments and short tubules (B), collapsed net (C), spread net (D), or partial net (E). Numbers shown are percentages. The fragments and short tubules category encompasses a range of morphologies from completely fragmented (as shown in B) to a mixture of fragments and short tubules. (F–H) Still images from time-lapse movies showing fission events in *mdv1*Δ yeast treated with 200 μM latrunculin A. The boxed area in the first frame is magnified in the subsequent sequence of five images. Arrows indicate fission events. Mitochondria were visualized with the outer membrane marker OM45–GFP. Bars, 1 μm.

### D.3.4 Mitochondrial Fission is Blocked by Overexpression of Caf4p or Caf4p Fragments

Because overexpression of Mdv1p or Mdv1p fragments inhibits mitochondrial fission Smirnova et al. (2001), we next tested the effects of Caf4p overproduction. Caf4p-HA under the control of the GalL promoter was expressed  $\approx 20$  times above endogenous levels in rich galactose medium (unpublished data). Spread mitochondrial nets formed in 23.5% cells (fig. D.5C). An additional 38% of cells had an intermediate phenotype that we termed “connected tubules,” consisting of a completely interconnected mitochondrial network in which no tubular ends were detected (fig. D.5B). Overexpression of an NH<sub>2</sub>-terminal fragment that interacts with Fis1p (residues 1–250; unpublished data) had a similar effect (9% spread nets, 33% connected tubules; fig. D.5), suggesting that the formation of mitochondrial net-like structures may result from a dominant-negative effect on Fis1p function. A similar distribution of mitochondrial phenotypes resulted from 20-fold overproduction of Mdv1p-HA (7.5% spread nets and 24.5% interconnected tubules) and an Mdv1p-HA NH<sub>2</sub>-terminal fragment (5% spread nets and 39% interconnected tubules; unpublished data). These data confirm that Caf4p interacts with the mitochondrial fission apparatus.

### D.3.5 Full Bypass Suppression of *fzo1* $\Delta$ Requires Loss of Both *MDV1* and *CAF4*

Yeast fission mutants are able to suppress the glycerol growth defect of cells deficient in mitochondrial fusion (Bleazard et al. 1999). Indeed, *MDV1* was originally identified because of its ability to suppress the glycerol growth defect of strains

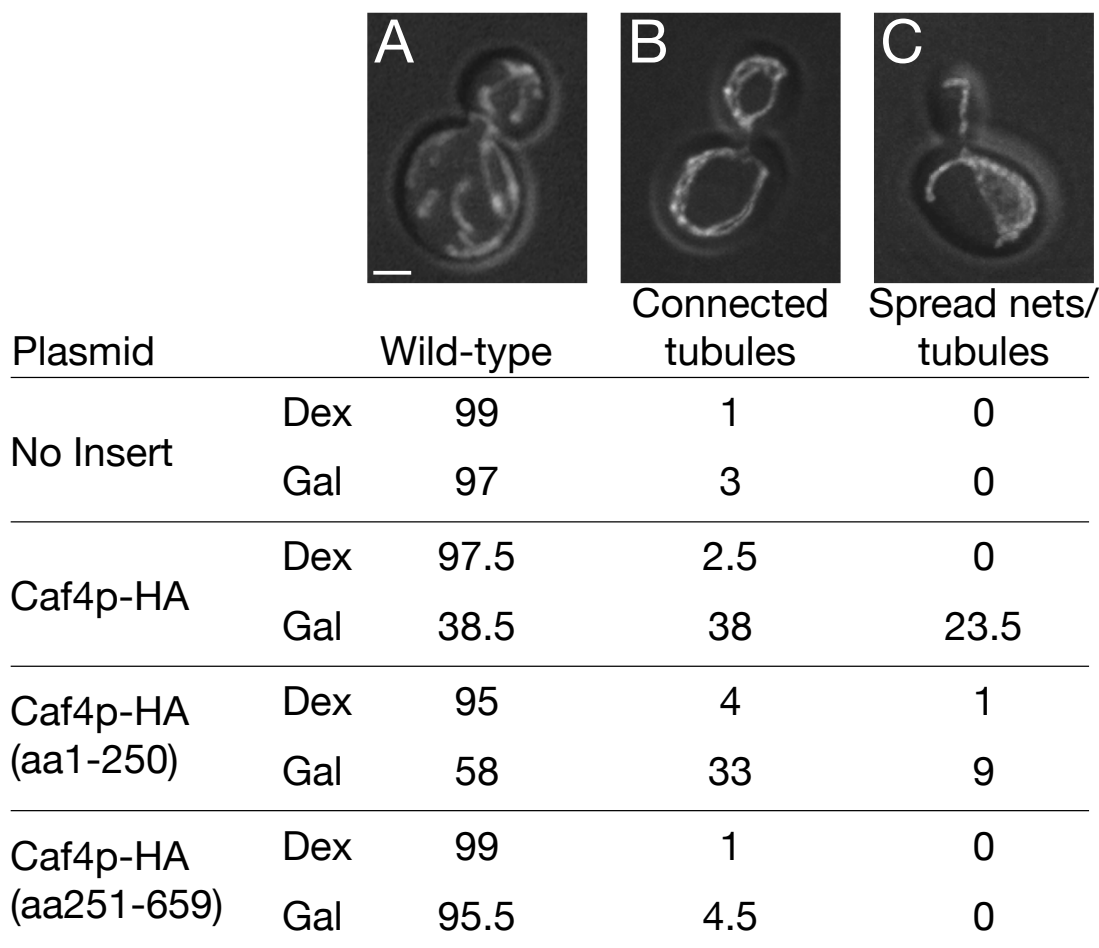


**Figure D.5 Caf4p Overexpression Blocks Mitochondrial Fission.** Wild-type yeast (DCY 1979) carrying the pRS 416 GalI vector with no insert, full-length CAF4-HA, CAF4-HA N, or CAF4-HA C were grown in rich dextrose or galactose media for 180 min and fixed. Cells were scored into the following phenotypic categories: wild-type (A), connected tubules (B), or spread nets with tubules (C). Numbers shown are percentages ( $n = 200$ ). Overexpression in galactose cultures was estimated to result in 20-fold greater expression than endogenous levels by Western blots of serially diluted lysates (not depicted). Bar, 1  $\mu$ m.

carrying temperature-sensitive *fzo1* or *mgm1* alleles (Fekkes et al. 2000; Mozdy et al. 2000; Tieu and Nunnari 2000; and Cervený et al. 2001). Deletion of *MDV1* has previously been reported to suppress the glycerol growth defect of *fzo1* $\Delta$  cells less efficiently than deletion of *DNM1* (Cervený et al. 2001). To further test our hypothesis that *mdv1* $\Delta$  cells have only a partial loss of mitochondrial fission, we compared



the efficiencies with which the *mdv1* $\Delta$  and *dnm1* $\Delta$  mutations suppress the glycerol growth defect of *fzo1* $\Delta$  cells. Diploids were sporulated, genotyped, and scored by serial dilution for their ability to grow on glycerol plates relative to dextrose plates (fig. D.6). As expected, all wild-type and no *fzo1* $\Delta$  spores grew on glycerol plates. Of 17 *mdv1* $\Delta$  *fzo1* $\Delta$  spores tested, 7 showed no detectable growth on glycerol and an additional 4 spores grew very poorly, with  $< 1\%$  cell survival on glycerol. Only 3 of the 6 remaining spores showed  $> 20\%$  survival on glycerol. More than half of *dnm1* $\Delta$  *fzo1* $\Delta$  spores grew robustly on glycerol plates, with between 20% and 50% cell survival. Most importantly, the triple mutant *mdv1* $\Delta$  *caf4* $\Delta$  *fzo1* $\Delta$  spores grew much more robustly than the *mdv1* $\Delta$  *fzo1* $\Delta$  spores, with all spores growing on glycerol and the majority between 20% and 50% cell survival. The markedly enhanced bypass suppression of *fzo1* $\Delta$  by *mdv1* $\Delta$  *caf4* $\Delta$  double mutations compared with the *mdv1* $\Delta$  mutation provides genetic evidence that *mdv1* $\Delta$  cells retain residual mitochondrial fission due to the activity of Caf4p.

### D.3.6 Caf4p Localizes to Mitochondria in a Fis1p-dependent Manner

We next sought to determine the subcellular localization of Caf4p. Caf4p was detected in highly purified mitochondrial preparations (Sickmann et al. 2003), and a Caf4p-GFP fusion generated in a genome-wide analysis localizes to mitochondria (Sickmann et al. 2003). We confirmed the mitochondrial localization of Caf4p-GFP, but did not study it further because the GFP fusion protein was not functional when expressed from the *CAF4* locus (unpublished data). We instead used immunofluorescence to localize Myc-tagged versions of Caf4p and Mdv1p (termed Caf4p-HTM and Mdv1p-HTM) that are expressed from the endogenous locus and are functional.

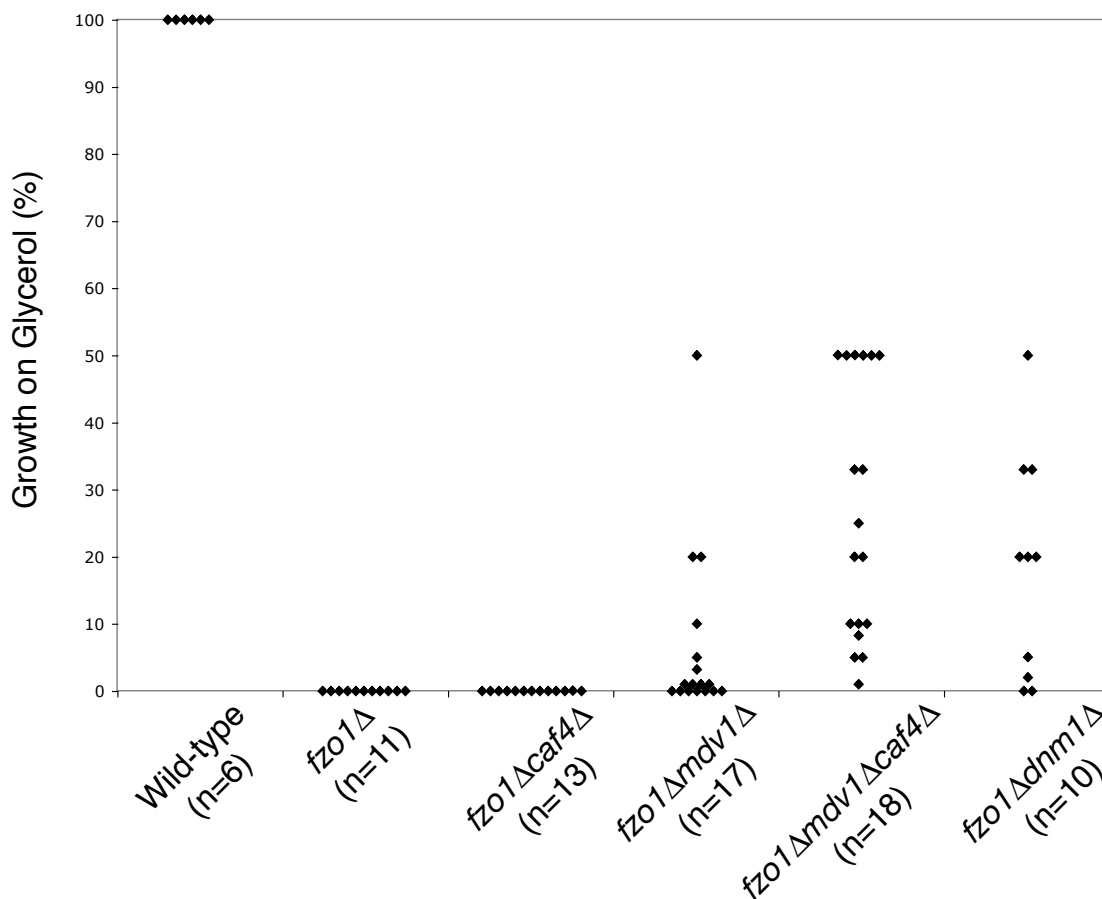


**Figure D.6 Suppression of the Glycerol Growth Defect of *fzo1Δ* Cells.** Individual spores of the indicated genotypes were assayed by serial dilution on YP glycerol and YP dextrose plates to determine the percent survival on glycerol-containing medium. Each point represents the viability of an individual spore. For clarity, spores showing 1% or less survival were plotted as 1%.

Caf4p-HTM and Mdv1p-HTM showed clear mitochondrial localization (fig. D.7). When cells were grown in rich dextrose medium, both Caf4p-HTM and Mdv1p-HTM displayed a largely uniform mitochondrial distribution with occasional areas of increased intensity. In rich galactose medium, Caf4p-HTM and Mdv1p-HTM localize in a more punctate pattern on mitochondria (fig. D.7, M–R). Caf4p-HTM partially colocalizes with Dnm1-GFP puncta (fig. D.7, S–U). In *fis1Δ* cells grown in either dextrose or galactose media, both Caf4p-HTM and Mdv1p-HTM are found

predominantly in the cytosol (fig. D.7, D–F and J–L). In some cells, however, low levels of residual localization to mitochondria could be discerned (e. g., fig. D.7, D–F). In *fis1* mutant yeast, overexpressed GFP–Mdv1p is diffusely cytosolic but also retains some localization to mitochondria (Tieu and Nunnari 2000; and Tieu et al. 2002). Together, these data indicate that the normal mitochondrial localization of both Caf4p and Mdv1p depends largely on Fis1p, although some low levels of residual localization can occur in the absence of Fis1p.

We also evaluated the localization of Caf4p–HTM by subcellular fractionation. We found a significant portion of both Caf4p and Mdv1p in the mitochondrial pellet (fig. D.7V). Mdv1p had previously been shown to be present in mitochondrial fractions (Fekkes et al. 2000; Tieu and Nunnari 2000; and Cervený et al. 2001). However, in *fis1*Δ yeast both proteins behave as cytosolic proteins (fig. D.7V). These data support our immunofluorescence studies and confirm that Mdv1p and Caf4p localize to mitochondria through their association with Fis1p.

### D.3.7 Caf4p Recruits Dnm1p–GFP to Mitochondria

To understand the mechanism of mitochondrial fission, it is crucial to elucidate how Dnm1p is recruited to mitochondria. Given that Mdv1p associates with both Fis1p and Dnm1p, it is puzzling that Dnm1p assembly on mitochondria shows little or no dependence on Mdv1p (Fekkes et al. 2000; Mozdy et al. 2000; Tieu and Nunnari 2000; Tieu et al. 2002; and Cervený and Jensen 2003). With the identification of Caf4p as a component of the fission machinery, we reexamined this issue. We constructed a fully functional Dnm1p–GFP allele and analyzed its localization pattern using deconvolution microscopy (Table D.9). Similar to previous reports

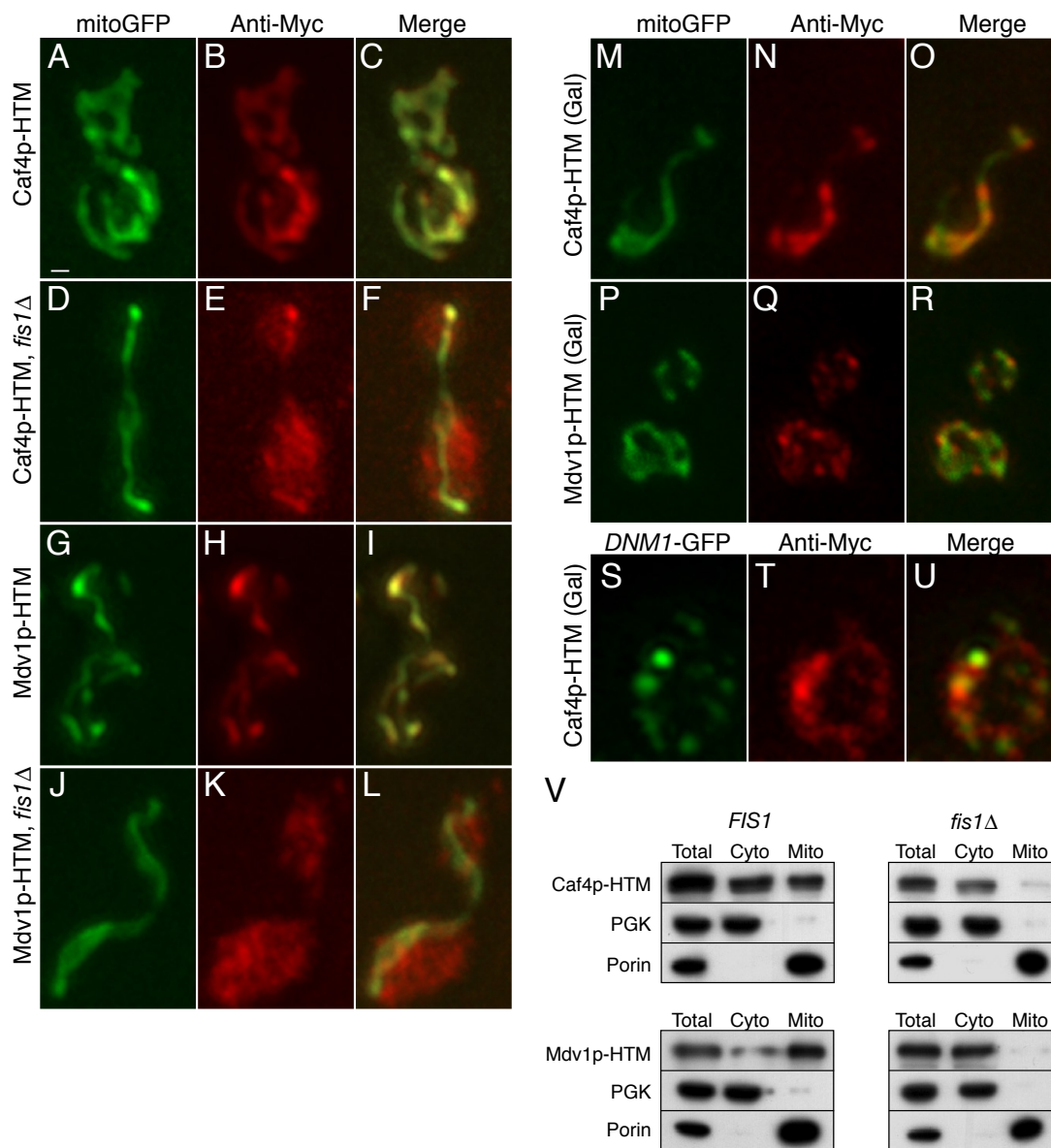


**Figure D.7 Mitochondrial Localization of Caf4p and Mdv1p Requires Fis1p.** Immunofluorescence (red, middle panels) was used to localize Myc-tagged Caf4p (Caf4p-HTM; A-F and M-U) and Mdv1p (Mdv1p-HTM; G-L and P-R) in wild-type (A-C, G-I, and M-U) and *fis1Δ* cells (D-F and J-L). Caf4p-HTM and Mdv1p-HTM are expressed from the endogenous loci and are functional. Mitochondria were labeled with mitochondrially targeted GFP (A-R, left, green). The majority of Dnm1p-GFP puncta colocalize with Caf4p-HTM (S-U). Overlays of the two signals are shown in the merged images (right). Note that both Caf4p and Mdv1p localize to mitochondria in wild-type cells, but are diffusely cytosolic in *fis1Δ* cells. Cells were grown in YP dextrose (A-L) or YP galactose (M-U). Representative maximum intensity projections of deconvolved z-stacks are shown. Bar, 1  $\mu$ m. (V) Caf4p-HTM and Mdv1p-HTM were analyzed by subcellular fractionation. The total cell lysate (Total), high-speed supernatant (Cyto), and mitochondrial pellet (Mito) were analyzed by Western blot with an anti-Myc antibody in wild-type (left) and *fis1Δ* (right) yeast. PGK (3-phosphoglycerate kinase) is a cytosolic marker, and porin is a mitochondrial outer membrane marker.

**Table D.9 Quantification of Dnm1–GFP Puncta Localization.** Dnm1p puncta were scored for colocalization with mitochondrially localized DsRed in deconvolved images. For each genotype, 140 budded cells were analyzed by scoring Dnm1p–GFP spots in both the mother and bud, and the average is presented with the SD in parentheses.

	Mitochondrial	Cytosolic
Wild-type	16.9 ( $\pm 5.5$ )	3.3 ( $\pm 2.1$ )
<i>caf4</i> $\Delta$	15.4 ( $\pm 5.2$ )	5.2 ( $\pm 2.6$ )
<i>mdv1</i> $\Delta$	13.7 ( $\pm 5.0$ )	5.1 ( $\pm 3.0$ )
<i>fis1</i> $\Delta$	4.9 ( $\pm 2.7$ )	9.6 ( $\pm 4.3$ )
<i>mdv1</i> $\Delta$ <i>caf4</i> $\Delta$	4.8 ( $\pm 2.5$ )	10.4 ( $\pm 3.9$ )

(Otsuga et al. 1998), Dnm1p–GFP is found predominantly in puncta associated with mitochondria (average 16.9 mitochondrial vs. 3.3 cytosolic puncta per cell; Table D.9 and fig. D.7, A–C). Deletion of *CAF4* or *MDV1* alone had little effect on this localization (15.4 mitochondrial vs. 5.2 cytosolic and 13.7 mitochondrial vs. 5.1 cytosolic per cell, respectively; Table D.9 and fig. D.8, D–I). In all these strains, the Dnm1p puncta are relatively uniform in size and intensity.

In contrast, *fis1* $\Delta$  mutants showed dramatic defects, with the majority of the puncta now cytosolic (4.9 mitochondrial vs. 9.6 cytosolic) (Table D.9 and fig. D.8, J–L). As has been previously noted, a small fraction of Dnm1p still localizes to mitochondria in *fis1* $\Delta$  cells (Tieu et al. 2002; and Cervený and Jensen 2003), suggesting that Dnm1p may be recruited by a second pathway, perhaps through an intrinsic affinity for mitochondrial lipids or an unidentified mitochondrial binding partner. Importantly, a similar defect in Dnm1p localization was found in *mdv1* $\Delta$  *caf4* $\Delta$  cells (4.8 mitochondrial vs. 10.4 cytosolic per cell) (Table D.9 and fig. D.8, M–O). In both *fis1* $\Delta$  and *mdv1* $\Delta$  *caf4* $\Delta$  cells, Dnm1p–GFP forms a few large aggregates and numerous less intense puncta. Similar results were obtained using immunofluorescence against a Dnm1p–HTM protein (unpublished data). These data clearly demonstrate that either Caf4p or Mdv1p is sufficient for effective recruitment of

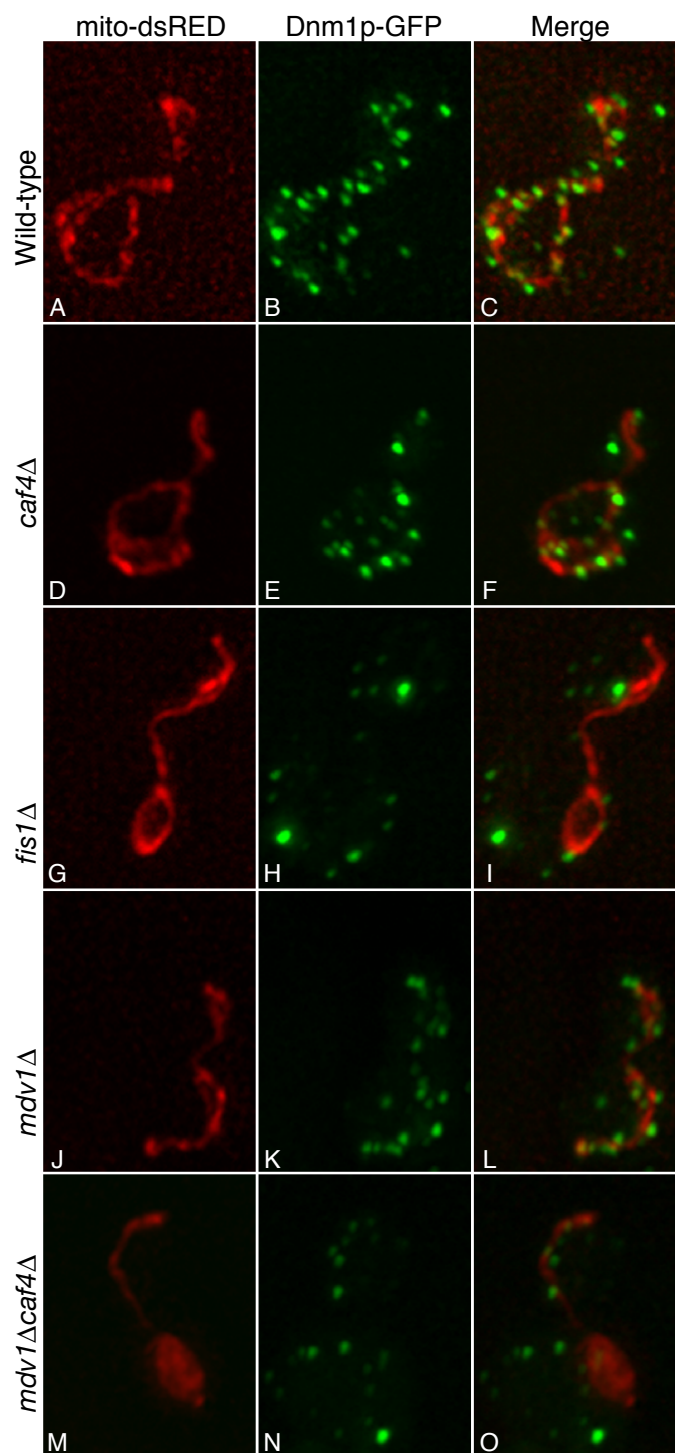


**Figure D.8 Fis1p Mediates Dnm1p-GFP Localization Through Either Mdv1p or Caf4p.** The localization of Dnm1p-GFP (middle, green) was compared to mito-DsRed (left, red) in yeast of the indicated genotype. Merged images are shown on the right. Representative maximum intensity projections of deconvolved z-stacks are shown.

Dnm1p to mitochondria, and that Caf4p is essential for Mdv1p-independent recruitment of Dnm1p by Fis1p.

## D.4 Discussion

### D.4.1 *CAF4* and *MDV1* Perform Similar Functions in Mitochondrial Fission

By applying affinity purification and mass spectrometry to Fis1p, we have identified Caf4p as a novel component of the mitochondrial fission machinery. Our biochemical and genetic characterization indicate that *CAF4* functions in the same manner as *MDV1* in mitochondrial fission. Biochemically, both proteins interact with Fis1p and Dnm1p. Caf4p and Mdv1p share a common domain architecture comprised of an NTE, a central CC, and a COOH-terminal WD40 repeat. The NH<sub>2</sub>-terminal regions mediate oligomerization and association with Fis1p, whereas the COOH-terminal WD40 regions mediate interactions with Dnm1p. In addition, both Caf4p and Mdv1p localize to mitochondria in a Fis1p-dependent manner.

Genetically, both *MDV1* and *CAF4* act positively in the mitochondrial fission pathway. *mdv1*Δ cells are dramatically compromised for mitochondrial fission, but a residual level of fission is mediated by *CAF4*. This residual fission activity is revealed by the observation that *mdv1*Δ yeast have a less severe mitochondrial morphology defect compared with *fis1*Δ or *dnm1*Δ yeast. In contrast, *mdv1*Δ *caf4*Δ yeast display predominantly collapsed mitochondrial nets, identical to those seen in *fis1*Δ and *dnm1*Δ cells. Time-lapse imaging of mitochondria in *mdv1*Δ cells indeed reveals a residual level of fission that is absent from *mdv1*Δ *caf4*Δ

cells. These results directly support our conclusion that the morphology differences between *mdv1* $\Delta$  cells versus *mdv1* $\Delta$  *caf4* $\Delta$ , *fis1* $\Delta$ , and *dnm1* $\Delta$  cells are primarily due to differences in fission rates. It is also possible that the proposed role of Dnm1p in cortical distribution of mitochondria may contribute in part to the morphological differences (Otsuga et al. 1998). The *mdv1* $\Delta$  mutation acts as a weak suppressor of the glycerol growth defect in *fzo1* $\Delta$  cells. The *mdv1* $\Delta$  *caf4* $\Delta$  double mutation suppresses this phenotype much more efficiently. Based on these physical interaction and genetic data, we conclude that Caf4p likely acts in a similar manner to Mdv1p to promote mitochondrial fission.

Why are there two proteins that appear to perform similar and partially redundant roles in mitochondrial fission? This question is particularly intriguing because *caf4* $\Delta$  yeast have normal mitochondrial morphology, indicating that disruption of Caf4p does not cause a major loss of mitochondrial fission. First, *CAF4* may play a more important role in mitochondrial fission under conditions not yet tested. Second, the presence of two proteins mediating interactions between Fis1p and Dnm1p would increase the ability of cells to accurately regulate the rate of mitochondrial fission. The heterotypic and homotypic interactions between Caf4p and Mdv1p may provide an additional layer of regulation. Finally, Caf4p may have an additional function in another pathway. Previous two-hybrid studies have implicated Caf4p in the CCR4-NOT complex, which is thought to be involved in regulation of transcription and/or mRNA processing (Liu et al. 2001).

#### D.4.2 A Revised Model for Mitochondrial Fission

The current models for mitochondrial fission propose that Mdv1p acts late in the



fission pathway. One model proposes a two-step pathway in which Fis1p first recruits Dnm1p, in an Mdv1p-independent manner. Mdv1p then acts as a molecular adaptor at a postrecruitment step, along with Fis1p, to promote fission by Dnm1p (Shaw and Nunnari 2002; Tieu et al. 2002; and Osteryoung and Nunnari 2003). A second model also proposes that Mdv1p acts after Dnm1p recruitment to organize an active fission complex (Cervený and Jensen 2003).

Our study reveals a new role for Mdv1p and Caf4p early in mitochondrial fission. Fis1p recruits Dnm1p to mitochondrial fission complexes through Mdv1p or Caf4p, which act as molecular adaptors. This revised model is strongly supported by our demonstration that Dnm1p recruitment in *mdv1* $\Delta$  yeast depends on Caf4p function. In the absence of both Mdv1p and Caf4p, Fis1p is unable to recruit Dnm1p.

Although Mdv1p and Caf4p clearly act early in the fission pathway, there is evidence that at least Mdv1p has a subsequent role in the activation of fission, as previously proposed (Shaw and Nunnari 2002; Tieu et al. 2002; and Cervený and Jensen 2003). In *caf4* $\Delta$  cells, Mdv1p recruits Dnm1p to fission complexes, and fission occurs at apparently normal levels. However, in *mdv1* $\Delta$  cells, Caf4p is similarly able to recruit Dnm1p to fission complexes, but mitochondrial fission is severely compromised. Therefore, Mdv1p and Caf4p can independently recruit Dnm1p, but complexes recruited by Mdv1p appear to be more highly active. These observations suggest that Dnm1p recruitment by itself is insufficient for fission to occur. Indeed, studies of Dnm1p dynamics indicates that most Dnm1p puncta do not result in fission (Legesse-Miller et al. 2003). Our identification of Caf4p as part of the fission machinery clarifies the early steps in mitochondrial fission. Future studies will need to define the additional steps beyond Dnm1p recruitment necessary for fission.

## D.5 Materials and Methods

### D.5.1 Media and Yeast Genetic Techniques

Yeast strains are listed in Table S1. Standard genetic techniques and yeast media were used. SC and YP media supplemented with either 2% dextrose, 3% glycerol, 2% raffinose, or 2% galactose were prepared as described previously (Guthrie and Fink 1991). YJG 12 and DCY 1557 are in the W303 background. All other strains are in the S288C background. *fis1::KanMX6*, *mdv1::KanMX6*, *caf4::KanMX6*, and *dnm1::KanMX6* are derived from the *MATa* deletion library (Open Biosystems).

### D.5.2 Plasmid Construction

The M<sub>9</sub>TH cassette was generated as follows. Primers Eg 258 (see Table S3, available at <http://www.jcb.org/cgi/content/full/jcb.200503148/DC1>) and Eg 259 were used to amplify *URA3* from pRS 416 (Stratagene). Eg 260 and Eg 4, an *FZO1* reverse primer, were used to amplify a TEV/His<sub>8</sub> module from EG 704 (pRS 414+9×Myc/TEV/His<sub>8</sub>-*FZO1*). The 3' end of the *URA3* product overlaps by 18 bp with the 5' end of the TEV/His<sub>8</sub> product. This overlap allows them to anneal together and be amplified in a second PCR with the primers Eg 258 and Eg 4. The *URA3*/TEV/His<sub>8</sub> product was cloned into pRS 403 as an EcoRV/SalI fragment (which removes all *FZO1* sequence), resulting in EG 928. 9×Myc/TEV was amplified with Eg 256 and Eg 260 from EG 704 and fused to the 5' end of *URA3* (Eg 258/259 product) by mixing and amplifying with Eg 256 and Eg 259. The

resulting product was cloned into EG 928 as an EcoRV/EcoRI fragment, yielding EG 940 (pRS 403+9×Myc/TEV/*URA3*/TEV/His<sub>8</sub>). EG 940 was converted to pRS 403+3×Myc/TEV/*URA3*/TEV/His<sub>8</sub> by digesting with Xba1, yielding EG 957.

To construct HA-tagged versions of *CAF4* and *CAF4* fragments, *CAF4* sequences were PCR amplified from *end3Δ* genomic DNA (Open Biosystems). First, the *CAF4* 3' untranslated region (UTR) was amplified with the primers Eg 313 and Eg 314 and cloned as a KpnI/SalI fragment into pRS 416, resulting in pRS 416+*CAF4* 3' UTR. 3×HA was amplified with Eg 327 and Eg 328 and cloned as a SalI/XhoI fragment into the SalI site to generate pRS 416+3×HA/*CAF4* 3' UTR. The *CAF4* 5' UTR was cloned as a SacI/SpeI fragment using Eg 312 and Eg 317, resulting in pRS 416+*CAF4* 5' UTR/3×HA/3' UTR. Full-length *CAF4* was amplified with Eg 316 and Eg 315 and cloned as a SpeI/XhoI fragment into the SpeI/SalI sites, resulting in EG 1041. *CAF4* N (residues 1–274) and C (residues 275–659) were amplified with Eg 316/Eg 353 and Eg 315/Eg 352, respectively, and cloned as SpeI/XhoI fragments, resulting in EG 1045 and EG 1043. Four independent clones encoded glutamine at residue 110 and arginine at residue 111. Full-length *CAF4*–HA was able to complement *caf4Δ* in *caf4Δ mdv1Δ* yeast, indicating that it is functional.

To construct HA-tagged versions of *MDV1* and *MDV1* fragments, *MDV1* sequences were amplified by PCR from *end3Δ* genomic DNA. First, the *MDV1* 3' UTR was amplified with the primers Eg 323 and Eg 324 and cloned as a SacI/SalI fragment into pRS 416. A 3×HA cassette was added as described for *CAF4*–HA, resulting in the plasmid pRS 416+3×HA–*MDV1* 3' UTR. The *MDV1* 5' UTR was amplified with primers Eg 320 and Eg 322 and cloned as a SacII/SpeI fragment, resulting in pRS 416+*MDV1* 5' UTR/3×HA/3' UTR. Full-length *MDV1* was amplified using primers Eg 109 and Eg 321 and cloned as a SpeI/XhoI fragment into the

SpeI/SalI sites, resulting in EG 1047. *MDV1* N (residues 1–300) and C (residues 301–714) were amplified with Eg 323/Eg 326 and Eg 321/325, respectively, and cloned as SpeI/XhoI fragments, resulting in EG 1051 and EG 1049. Full-length *MDV1*–HA complemented the mitochondrial morphology defects in *mdv1* $\Delta$  cells.

The galactose-inducible Caf4p expression vectors EG 1133 (Caf4p–HA), EG 1135 (Caf4p–HA, residues 251–659), and EG 1136 (Caf4p–HA, residues 1–250) were generated by replacing the *CAF4* 5' UTR in EG 1041, EG 1043, and EG 1045 with a SacI/ClaI GalL promoter fragment from p 413 GalL (Mumberg et al. 1994) containing a start codon inserted between the XbaI and EcoRI sites.

pRS 403+GPD/mito–GFP (EG 686) was generated by first cloning the GPD promoter from p 413 GPD (Mumberg et al. 1995) as a SacI (blunt)/SpeI fragment into the SmaI/SpeI sites of pRS 403 (Stratagene), yielding EG 128. Next, a HindIII (blunt)/NotI mito–GFP fragment from pYES–mtGFP (Westermann and Neupert 2000) was inserted into EG 128 linearized with SpeI (blunt)/NotI. pRS 403+GPD/mito–DsRed (EG 823) was generated by subcloning DsRed into the BamHI and NotI sites of EG 686, replacing GFP with DsRed. OM45 was PCR amplified with primers Eg 151 and Eg 154 and cloned as an XhoI/XbaI fragment with an XbaI/BamHI GFP fragment into the XhoI/BamHI sites of pRS 416, yielding pRS 416+OM45–GFP (EG 252).

### D.5.3 Yeast Strain Construction

An M<sub>9</sub>TH–*FIS1* strain was generated by amplifying the 9 $\times$ Myc/TEV/*URA3*/TEV/His<sub>8</sub> cassette from EG 943 (pRS 403–9 $\times$ Myc/TEV/*URA3*/TEV/His<sub>8</sub>) with the *FIS1*–targeting primers Eg 261 and Eg 262 and transforming YJG 12. *URA3*+ transfor-

ants were screened by PCR for correct integration (2 out of 8 positive), grown overnight in YPD to allow for loss of *URA3*, and plated on 5-FOA plates. Colonies were screened by Western blotting for expression of M<sub>9</sub>TH-Fis1p (9 out of 16 positive). This strain displayed wild-type morphology in 64 % of cells and moderate defects in the remaining cells. The same strategy was used to generate M<sub>3</sub>TH-*FIS1* from the pRS 403-3×Myc/TEV/*URA3*/TEV/His<sub>8</sub> template (EG 957) for subsequent experiments in the S288C background. This strain (DCY 2192) displayed wild-type morphology in 89 % of cells and mild defects in the remaining cells. DCY 2192 was crossed to *mdv1*Δ and *caf4*Δ strains (Open Biosystems *MATa* deletion library) and sporulated to generate M<sub>3</sub>TH-*FIS1 mdv1*Δ (DCY 2302) and M<sub>3</sub>TH-*FIS1 caf4*Δ (DCY 2305).

*fzo1::HIS5* was generated by transformation with a *HIS5* (*Saccharomyces kluyveri*) fragment amplified with the *FZO1* targeting primers Eg 9 and Eg 10. mito-GFP was integrated to the *leu2*Δ0 locus by transformation with NarI-digested EG 686 (pRS 403+GPD/mito-GFP). mito-DsRed was integrated to the *leu2*Δ0 locus by transformation with HpaI-digested EG 823 (pRS 403+GPD/mito-DsRed). *dnm1*Δ::*HIS5* was generated by transformation with a *HIS5* (*S. kluyveri*) fragment amplified with the *DNM1*-targeting primers Eg 57 and Eg 58.

Chromosomal *CAF4*-HTM was generated by transformation of DCY1979 with a His<sub>8</sub>/2TEV/9×Myc/*HIS5* cassette (Westermann and Neupert 2000) amplified with the *CAF4* targeting primers Eg 284 and Eg 285. Chromosomal *MDV1*-HTM was generated transformation with the same cassette amplified with *MDV1* targeting primers Eg 80 and Eg 81. Both *CAF4*-HTM and *MDV1*-HTM are functional because 70 % of *CAF4*-HTM *mdv1*Δ yeast display spread mitochondrial nets and 95 % of *MDV1*-HTM yeast cells display wild-type mitochondrial morphology.

*DNM1*-GFP was generated by amplifying GFP/*HIS5* from pKT 128 (Sheff and Thorn 2004) with Eg 342 and Eg 343. This product was transformed into DCY 1626 (wild-type yeast with mito-DsRed) to generate DCY 2370. DCY 2370 was crossed to *fis1* $\Delta$  and *mdv1* $\Delta$  *caf4* $\Delta$  strains to generate strains DCY 2404 (*DNM1*-GFP *fis1* $\Delta$ ), DCY 2414 (*DNM1*-GFP *caf4* $\Delta$ ), DCY 2417 (*DNM1*-GFP *mdv1* $\Delta$ ), and DCY 2418 (*DNM1*-GFP *mdv1* $\Delta$  *caf4* $\Delta$ ).

#### D.5.4 Tandem Affinity Purification MudPIT

Pellets from 2 l cultures ( $OD_{600\text{ nm}} \approx 1.5$ ) grown in YPD were prepared essentially as described previously for HPM tag Dual-Step affinity purification (Sheff and Thorn 2004), with the following modifications. Fungal protease inhibitors were used (Sigma-Aldrich) and lysates were cleared at 20 kg for 15 min. Cleavage from 9E10 beads was performed with GST-TEV protease for 3 h at RT. The second affinity step was performed with 40  $\mu$ l Magne-His beads (Promega). Samples were proteolytically digested and analyzed by multidimensional chromatography in-line with a Deca XP ion trap mass spectrometer (ThermoElectron) as described previously (Mayor et al. 2005). Samples were released stepwise from the strong cation exchanger phase of the triphasic capillary columns as reported previously (Mayor et al. 2005).

#### D.5.5 Immunoprecipitation

*CAF4*-HA (EG 1041), *CAF4*-HA residues 1-274 (EG 1043), and *CAF4*-HA residues 275-659 (EG 1045) were expressed in strains DCY 1979 (wild-type) and DCY 2305

( $M_3TH-FIS1\ caf4\Delta$ ).  $MDV1$ -HA (EG 1047),  $MDV1$ -HA residues 1–300 (EG 1049), and  $MDV1$ -HA residues 301–714 (EG 1051) were expressed in DCY1979 or DCY 2302 ( $M_3TH-FIS1\ mdv1\Delta$ ). Cultures were grown in selective SD media and harvested at  $OD_{600\text{ nm}} \approx 0.8$ . 20  $OD_{600\text{ nm}}$  units of cells were lysed with glass beads (40 s with a vortex mixer, 4 times) in 500  $\mu\text{l}$  ice-cold lysis buffer (50 mM Tris, pH 7.4, 150 mM NaCl, 0.1 mM EDTA, and 0.2% Triton X-100) in the presence of Fungal protease inhibitors (Sigma-Aldrich). Lysates were cleared by centrifuging 5 min at 5 krpm and 15 min at 14 krpm. At this point, a total lysate sample was taken. 400  $\mu\text{l}$  of cleared lysate was mixed with a 20  $\mu\text{l}$  bead volume of 9E10-conjugated protein A-Sepharose beads (Sigma-Aldrich) for 90 min. Beads were washed four times with 1 ml washes of lysis buffer. Precipitate was eluted with 100  $\mu\text{l}$  SDS buffer at 95°C for 5 min. SDS-PAGE Western blotting was performed with 9E10 hybridoma supernatant (anti-Myc) or 12CA5 ascites fluid (anti-HA).

### D.5.6 Yeast Two-hybrid Assay

pGAD vectors were transformed into PJ69-4 $\alpha$ . pGBDU vectors were transformed into PJ69-4a (James et al. 1996). Indicated vectors were mated on YPD plates using two transformants for each vector (totaling four matings per combination). Diploids were selected by replica plating to SD-leu-ura plates. Interactions were assayed by replica plating to SD-leu-ura-lys-ade and incubating for 4 d at 30°C.

### D.5.7 Mitochondrial Morphology Analysis

Mitochondrially targeted GFP (mito-GFP) was used to monitor mitochondrial morphology. DCY1979 (wild-type), DCY1945 ( $caf4\Delta$ ), DCY1984 ( $caf4\Delta\ mdv1\Delta$ ),

DCY 2009 (*fis1* $\Delta$ ), DCY 2128 (*mdv1* $\Delta$ ), DCY 2155 (*mdv1* $\Delta$  *dnm1* $\Delta$ ), and DCY 2312 (*dnm1* $\Delta$ ) were grown overnight, diluted 1:20 into fresh medium, and grown for 4 h at 30°C. Cultures were fixed by adjusting cultures to 3.7% formaldehyde and incubated 10 min at 30°C. Cells were washed 4 times with 1 ml PBS and scored for mitochondrial morphology. For *CAF4* overexpression studies, plasmids p416 GalL/*CAF4*-HA (EG 1133), p416 GalL/*CAF4*-HA residues 251–659 (EG 1135), or p416 GalL/*CAF4*-HA residues 1–250 (EG 1137) were transformed into DCY 1979. Cultures were grown overnight in selective SRaff and diluted 1:20 in fresh YPD or YPGal and grown 3 h at 30°C. Samples were taken for Western analysis and the remaining culture was fixed as described above.

For latrunculin A treatment, overnight YPD cultures were diluted 1:20 in fresh YPD and grown for 3 h. Cultures were then treated for 1 h at 30°C with 200  $\mu$ M latrunculin A in or with an equivalent amount of vehicle (DMSO). Cultures were then fixed as described above.

For time-lapse imaging, overnight SGal cultures were diluted 1:20 in fresh YPGal and grown for 3 h. Cells were pelleted, resuspended in fresh media, and embedded in 1% low melting point agarose containing 200  $\mu$ M latrunculin A.

### D.5.8 Bypass Suppression Assay

DCY 2002 and DCY 2343 were sporulated and dissected onto YPD plates. Spores were picked, grown overnight in 3 ml YPD at 30°C, pelleted, and resuspended to  $OD_{600\text{ nm}} \approx 1.0$  in YP. 3  $\mu$ l of 1:5 serial dilutions were spotted on YPD and YPGlycerol and grown at 30°C for 2 and 4 d, respectively, to determine the fraction of cells that grow on glycerol. Genotypes were determined by PCR.



### D.5.9 Differential Centrifugation

Yeast strains *CAF4*-HTM (DCY 2055), *CAF4*-HTM *fis1* $\Delta$  (DCY 2094), *MDV1*-HTM (DCY 2053), and *MDV1*-HTM *fis1* $\Delta$  (DCY 2097) were grown in YPD and harvested at  $OD_{600\text{ nm}} \approx 1.2$ . 100 OD units of cells were spheroplasted with zymolyase and lysed in a small clearance Dounce homogenizer (0.6 M sorbitol and 100 mM Tris, pH 7.4). The lysate was spun twice at 2.9 krpm for 5 min. An aliquot of the second supernatant was saved as the total lysate sample. The second supernatant was spun at 10 krpm for 10 min, and an aliquot of the supernatant was saved as the cytosol sample. The pellet was resuspended and spun again at 10 krpm for 10 min. An aliquot of the final pellet was saved as the mitochondrial pellet. Equal cell equivalents were loaded for Western blot analysis. The difference in porin intensity between the total and mitochondrial fractions most likely results from fewer obscuring proteins in the mitochondrial fraction.

### D.5.10 Imaging

Images were acquired on a microscope (Axiovert 200M; Carl Zeiss MicroImaging, Inc.) using a 100 $\times$  Plan-Apochromat, NA 1.4, oil-immersion objective. Z-stack images (between 0.1 and 0.2  $\mu\text{m}$  intervals for still images and between 0.3 and 0.4  $\mu\text{m}$  intervals for time-lapse images) were collected at RT with an ORCA-ER camera (Hamamatsu), controlled by AxioVision 4.2 software. Images were collected at either 30 or 40 s intervals for 30 min for time-lapse experiments. Iterative deconvolutions were performed with Axiovision 4.2 and maximum intensity projections were generated with AxioVision 4.2 for still images and Image J for time-lapse images.

Fluorescent images in Figs. D.3–D.5 were overlaid with differential interference contrast images (set at 50 % opacity) in Adobe Photoshop CS.

### D.5.11 Immunofluorescence

Cells were processed for immunofluorescence essentially as described previously (Guthrie and Fink 1991) with the following modifications. Cultures were fixed for 15 min with 3.7 % formaldehyde. Tween 20 (0.5 %) was included in blocking buffer (PBS, 1 % BSA) during a 15 min block step. Cells were stained with 9E10 hybridoma supernatant and a Cy3-conjugated anti-mouse secondary antibody. Washes after primary and secondary incubations were 5 min with blocking buffer, 5 min with blocking buffer containing 0.5 % Tween 20, and two 5 min washes with blocking buffer. All incubations were performed at RT. GelMount (Biomed) was used as mounting medium to preserve fluorescence.

### D.5.12 Online supplemental material

Table S1 lists proteins identified in MudPIT experiments with M<sub>9</sub>TH-Fis1p. Table S2 shows yeast strains. Table S3 lists primer sequences. Videos 1 and 2 show mitochondrial fission in *mdv1*Δ yeast. Mitochondria were monitored by the mitochondrial outer membrane marker OM45-GFP. Arrows highlight a subset of fission events. Online supplemental material available at <http://www.jcb.org/cgi/content/full/jcb.200503148/DC1>.

## D.6 Acknowledgments

We thank T.R. Suntok, S.A. Detmer, and H. Chen for helpful comments on the manuscript; and L. Lytle for technical assistance. J. Copeland constructed some of the two-hybrid plasmids. We thank Dr. Ray Deshaies for stimulating discussions on mass spectrometry.

E.E. Griffin was supported by a National Institutes of Health training grant (NIH GM07616) and a Ferguson fellowship. MudPIT analysis was performed in the mass spectrometry facility of the laboratory of R.J. Deshaies (Investigator, Howard Hughes Medical Institute, Caltech). This facility is supported by the Beckman Institute at Caltech and by a grant from the Department of Energy to R.J. Deshaies and B.J. Wold. J. Graumann is supported by R.J. Deshaies through Howard Hughes Medical Institute funds. D.C. Chan is a Bren Scholar and Beckman Young Investigator. This research was supported by the National Institutes of Health (GM62967).

## D.7 References

Bleazard, W., McCaffery, J. M., King, E. J., Bale, S. and Mozdy, A. et al. (1999).

The dynamin-related GTPase Dnm1 regulates mitochondrial fission in yeast. *Nat Cell Biol*, 1(5):298–304.

Boldogh, I., Vojtov, N., Karmon, S. and Pon, L. A. (1998). Interaction between

mitochondria and the actin cytoskeleton in budding yeast requires two integral mitochondrial outer membrane proteins, Mmm1p and Mdm10p. *J Cell Biol*, 141(6):1371–81.

- Cervený, K. L. and Jensen, R. E. (2003). The WD-repeats of Net2p interact with Dnm1p and Fis1p to regulate division of mitochondria. *Mol Biol Cell*, 14(10):4126–39.
- Cervený, K. L., McCaffery, J. M. and Jensen, R. E. (2001). Division of mitochondria requires a novel DMN1-interacting protein, Net2p. *Mol Biol Cell*, 12(2):309–21.
- Denis, C. L. and Chen, J. (2003). The CCR4–NOT complex plays diverse roles in mRNA metabolism. *Prog Nucleic Acid Res Mol Biol*, 73:221–50.
- Dimmer, K. S., Fritz, S., Fuchs, F., Messerschmitt, M. and Weinbach, N. et al. (2002). Genetic basis of mitochondrial function and morphology in *Saccharomyces cerevisiae*. *Mol Biol Cell*, 13(3):847–53.
- Fannjiang, Y., Cheng, W. C., Lee, S. J., Qi, B. and Pevsner, J. et al. (2004). Mitochondrial fission proteins regulate programmed cell death in yeast. *Genes Dev*, 18(22):2785–97.
- Fekkes, P., Shepard, K. A. and Yaffe, M. P. (2000). Gag3p, an outer membrane protein required for fission of mitochondrial tubules. *J Cell Biol*, 151(2):333–40.
- Frank, S., Gaume, B., Bergmann-Leitner, E. S., Leitner, W. W. and Robert, E. G. et al. (2001). The role of dynamin-related protein 1, a mediator of mitochondrial fission, in apoptosis. *Dev Cell*, 1(4):515–25.
- Griffin, E. E., Graumann, J. and Chan, D. C. (2005). The WD40 protein Caf4p is a component of the mitochondrial fission machinery and recruits Dnm1p to mitochondria. *J Cell Biol*, 170(2):237–48.
- Guthrie, C. and Fink, G. (1991). *Guide to Yeast Genetics and Molecular Biology*, pages 933. Academic Press, San Diego, CA.

- Jagasia, R., Grote, P., Westermann, B. and Conradt, B. (2005). DRP-1-mediated mitochondrial fragmentation during EGL-1-induced cell death in *C. elegans*. *Nature*, 433(7027):754–60.
- James, P., Halladay, J. and Craig, E. A. (1996). Genomic libraries and a host strain designed for highly efficient two-hybrid selection in yeast. *Genetics*, 144(4):1425–36.
- Jensen, R. E., Hobbs, A. E., Cervený, K. L. and Sesaki, H. (2000). Yeast mitochondrial dynamics: Fusion, division, segregation, and shape. *Microsc Res Tech*, 51(6):573–83.
- Legesse-Miller, A., Massol, R. H. and Kirchhausen, T. (2003). Constriction and Dnm1p recruitment are distinct processes in mitochondrial fission. *Mol Biol Cell*, 14(5):1953–63.
- Liu, H. Y., Chiang, Y. C., Pan, J., Chen, J. and Salvatore, C. et al. (2001). Characterization of CAF4 and CAF16 reveals a functional connection between the CCR4-NOT complex and a subset of SRB proteins of the RNA polymerase II holoenzyme. *J Biol Chem*, 276(10):7541–8.
- Mayor, T., Lipford, J., Graumann, J., Smith, G. and Deshaies, R. (2005). Analysis of polyubiquitin conjugates reveals that the rpn10 substrate receptor contributes to the turnover of multiple proteasome targets. *Mol Cell Proteomics*, 4(6):741–51.
- Mozdy, A. D., McCaffery, J. M. and Shaw, J. M. (2000). Dnm1p GTPase-mediated mitochondrial fission is a multi-step process requiring the novel integral membrane component Fis1p. *J Cell Biol*, 151(2):367–80.

- Mumberg, D., Muller, R. and Funk, M. (1994). Regulatable promoters of *Saccharomyces cerevisiae*: comparison of transcriptional activity and their use for heterologous expression. *Nucleic Acids Res*, 22(25):5767–8.
- Mumberg, D., Muller, R. and Funk, M. (1995). Yeast vectors for the controlled expression of heterologous proteins in different genetic backgrounds. *Gene*, 156(1):119–22.
- Osteryoung, K. W. and Nunnari, J. (2003). The division of endosymbiotic organelles. *Science*, 302(5651):1698–704.
- Otsuga, D., Keegan, B. R., Brisch, E., Thatcher, J. W. and Hermann, G. J. et al. (1998). The dynamin-related GTPase, Dnm1p, controls mitochondrial morphology in yeast. *J Cell Biol*, 143(2):333–49.
- Praefcke, G. J. and McMahon, H. T. (2004). The dynamin superfamily: Universal membrane tubulation and fission molecules?. *Nat Rev Mol Cell Biol*, 5(2):133–47.
- Sesaki, H. and Jensen, R. E. (1999). Division versus fusion: Dnm1p and Fzo1p antagonistically regulate mitochondrial shape. *J Cell Biol*, 147(4):699–706.
- Shaw, J. M. and Nunnari, J. (2002). Mitochondrial dynamics and division in budding yeast. *Trends Cell Biol*, 12(4):178–84.
- Sheff, M. A. and Thorn, K. S. (2004). Optimized cassettes for fluorescent protein tagging in *Saccharomyces cerevisiae*. *Yeast*, 21(8):661–70.
- Sickmann, A., Reinders, J., Wagner, Y., Joppich, C. and Zahedi, R. et al. (2003). The proteome of *Saccharomyces cerevisiae* mitochondria. *Proc Natl Acad Sci USA*, 100(23):13207–12.

- Smirnova, E., Griparic, L., Shurland, D. L. and van der Bliek, A. M. (2001). Dynamin-related protein Drp1 is required for mitochondrial division in mammalian cells. *Mol Biol Cell*, 12(8):2245–56.
- Tieu, Q. and Nunnari, J. (2000). Mdv1p is a WD repeat protein that interacts with the dynamin-related GTPase, Dnm1p, to trigger mitochondrial division. *J Cell Biol*, 151(2):353–66.
- Tieu, Q., Okreglak, V., Naylor, K. and Nunnari, J. (2002). The WD repeat protein, Mdv1p, functions as a molecular adaptor by interacting with Dnm1p and Fis1p during mitochondrial fission. *J Cell Biol*, 158(3):445–52.
- Westermann, B. and Neupert, W. (2000). Mitochondria-targeted green fluorescent proteins: convenient tools for the study of organelle biogenesis in *Saccharomyces cerevisiae*. *Yeast*, 16(15):1421–7.
- Wolf, E., Kim, P. S. and Berger, B. (1997). MultiCoil: A program for predicting two- and three-stranded coiled coils. *Protein Sci*, 6(6):1179–89.

## About this Document

This document was typeset in Computer Modern (Knuth 1986), using ConTeXt (Hagen 2001), a modern L<sup>A</sup>T<sub>E</sub>X–analogous (Lamport 1994) macro package around the document typesetting language pdfT<sub>E</sub>X (Thanh 1998), an extension to T<sub>E</sub>X by Knuth (1984) capable of producing Adobe’s *portable document format* (pdf, Adobe Systems Incorporated 2004).

J. G.’s experience in maintaining parallel manuscript versions in pdfT<sub>E</sub>Xed high quality (submission to review) on the one hand and MicroSoft Word–readable format (collaborator interaction, final submission for the majority of biological journals) on the other hand was unpleasant (Graumann et al. 2004, chapter 2, was written with two code bases). ConTeXt’s capability of interpreting *extensible markup language* (XML, Yergeau et al. 2004) in combination with the XML import functionality provided by OpenOffice (<http://www.openoffice.org>) present a way out of source duplicity: pdfT<sub>E</sub>Xed (ConTeXted) and OpenOffice documents (exportable to MicroSoft Word) from one XML source.

J. G.’s ongoing C<sub>o</sub>nT<sub>E</sub>X<sub>M</sub>L project seeks to provide a set of XML entities suitable for scientific publication as well as corresponding stylesheets mapping the resulting XML code into ConTeXt and OpenOffice. This document is entirely coded in XML, implying that the ConTeXt–mapping style sheet is fairly complete at the time of writing. The OpenOffice specific stylesheet is present in rudiments and still under development.



## References

- Adobe Systems Incorporated (2004). *PDF Reference—Adobe Portable Document Format, Version 1.6.* , 5th edition.
- Graumann, J., Dunipace, L. A., Seol, J. H., McDonald, W. H. and Yates III, J. R. et al. (2004). Applicability of tandem affinity purification MudPIT to pathway proteomics in yeast. *Mol Cell Proteomics*, 3(3):226–37.
- Hagen, H. (2001). *ConTeXt, The Manual.* PRAGMA ADE, Hasselt, The Netherlands.
- Knuth, D. E. (1986). *Computers & Typesetting, Volume E: Computer Modern Typefaces.* Addison–Wesley Longman Publishing Co., Boston, MA, USA.
- Knuth, D. E. (1984). *Computers & Typesetting, Volume A: The TeXbook.* Addison–Wesley Longman Publishing Co., Boston, MA, USA.
- Lamport, L. (1994). *LaTeX, a Document Preparation System.* Addison–Wesley, 2nd edition.
- Thanh, H. T. (1998). The pdfTeX Program. *Cahiers GUTenberg*, pages 197–210.
- Yergeau, F., Cowan, J., Bray, T., Paoli, J. and Sperberg-McQueen, C. M. et al. (2004). XML 1.1, W3C Recommendation.

